International Journal of Pharmaceutics 666 (2024) 124820

Contents lists available at ScienceDirect

International Journal of Pharmaceutics

journal homepage: www.elsevier.com/locate/ijpharm

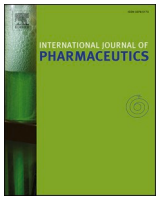

Mechanisms of dissolution and crystallization of amorphous glibenclamide

Vladimir Petkov, Zahari Vinarov *, Slavka Tcholakova

Department of Chemical and Pharmaceutical Engineering, Faculty of Chemistry and Pharmacy, Sofia University, 1 James Bourchier ave., 1164 Sofia, Bulgaria

ARTICLE INFO

Keywords:
Supersaturation
Formulation
Solubility
Wetting
Solubilization
Crystallization inhibition
polymer
cellulose

ABSTRACT

Amorphous solid dispersions enhance the dissolution and oral bioavailability of poorly water-soluble drugs. However, the link between polymer properties and formulation performance has not been fully clarified yet. We studied the effect of hydroxypropyl cellulose (HPC) polymers molecular weight (M_w) on the storage stability, dissolution kinetics and supersaturation stability of spray-dried amorphous glibenclamide (GLB) formulations. The solid-state stability of amorphous GLB during storage was significantly enhanced by both the 40 kDa (HPC-SSL) and 84 kDa (HPC-L) polymers, regardless of M_w differences. In contrast, HPC-SSL maintained significantly higher aqueous drug concentrations during dissolution, compared to HPC-L (its higher M_w analogue). Dedicated dissolution experiments, in situ optical microscopy and solid-state characterization revealed that aqueous drug concentrations were determined by the interplay between crystallization inhibition, drug ionization, wetting and solubilization effects: (1) HPC prevents surface nucleation, hence inhibiting crystallization, (2) intestinal colloids (bile salts and phospholipids) increase supersaturated drug concentrations via wetting and solubilization effects and (3) pH and drug ionization severely impact the degree of supersaturation. The better performance of the lower M_w HPC-SSL was due to its superior inhibition of surface crystallization during dissolution. These insights into the molecular mechanisms of dissolution and crystallization of amorphous solids provide foundation for rational formulation development.

1. Introduction

Many modern drugs exhibit poor aqueous solubility, which leads to low or highly variable oral bioavailability. One of the approaches to overcome this issue is the preparation of amorphous solid dispersions (ASD), in which amorphous drug is dispersed in solid polymer vehicle (Boyd, 2019; Dedroog et al., 2019; Singh and Van den Mooter, 2016). This offers better wettability and dispersibility for the drug, as well as a fast dissolution that usually leads to generation of supersaturated solutions and increased oral bioavailability.

Polymer selection, drug-to-polymer ratio and processing methods (spray drying, hot-melt extrusion, freeze-drying, cryo-milling), are the main aspects considered when aiming for long-term stability of the amorphous drug during storage, rapid drug dissolution and sustained supersaturation (Alonzo, 2011; Alonzo, 2010; Konno, 2008; Konno and Taylor, 2006; Grohganz, 2014; Knopp, 2016; Laitinen, 2013). In most cases, various types of cellulose derivates such as hydroxypropyl methylcellulose (Chavan, 2019; Li, 2010; Chavan et al., 2018) and hydroxypropyl methylcellulose acetate succinate are used as polymer vehicles (Butreddy, 2022; Corrie, 2023; Butreddy, 2022). Other types of polymers like polyvinylpyrrolidone (PVP) (Kestur, 2010; Mohapatra, 2017; Knopp, 2015) are also used as polymer vehicles. Polymers with different chemical properties are known to be able to stabilize the amorphous state of various drugs as well as providing additional protection against crystallization during supersaturation either by inhibiting nucleation or crystal growth. The known mechanisms of crystallization inhibition by polymers have been linked to intermolecular interactions such as hydrogen bonding and hydrophobic effects (Mukesh, 2023; Shan, 2021; Wu and Mooter, 2023).

When selecting a polymer for ASD preparation, apart from the chemistry (cellulose-based, PVP-based, other), the molecular weight (M_w) also has to be considered. For PVP, there is substantial experimental evidence that higher M_w species increase both the solid-state and supersaturated solution stability (Kestur, 2010; Mohapatra, 2017; Knopp, 2015). Although the mechanisms are not entirely clear, it is suggested that the increased solid-state stability is due to reduced mobility of the drug molecules when they are dispersed between longer polymer chains, whereas the sustained supersaturation is attributed to

* Corresponding author at: Department of Chemical and Pharmaceutical Engineering, Faculty of Chemistry and Pharmacy, Sofia University "St. Kl. Ohridski", 1 James Bourchier ave., 1164 Sofia, Bulgaria.
E-mail address: zv@lcpe.uni-sofia.bg (Z. Vinarov).

https://doi.org/10.1016/j.ijpharm.2024.124820
Received 4 July 2024; Received in revised form 4 October 2024; Accepted 9 October 2024
Available online 16 October 2024

classical crystal growth and/or nucleation inhibition.

However, recent studies on the effect of hydroxypropyl cellulose (HPC) M_w on ASD performance have revealed a more complex picture: lower M_w HPC were shown to enhance the solid-state stability of fenofibrate (Luebbert et al., 2021), whereas higher M_w HPC sustained better the supersaturation of celecoxib (Niederquell et al., 2022). These results suggest a drug- or polymer-specific nature of the M_w effect and have two important general implications: (1) the validity of the general mechanisms of the polymer M_w effects is questioned and (2) the impact of M_w of HPC polymers on ASD performance is unclear.

In order to gain more understanding on the effect of HPC M_w on ASD properties and the underlying mechanisms, we studied glibenclamide (GLB) ASD prepared by spray-drying and stabilized by HPC polymers (at 1:3 drug to polymer ratio) with different M_w. Dissolution of the spray dried powders was studied in biorelevant media (gastric and/or intestinal conditions), solid-state was monitored by microscopy, X-ray scattering and calorimetry. The mechanisms of the observed effects were studied by a set of dedicated experiments.

2. Materials and methods

2.1. Materials

GLB (99 %, Alfa Aesar) was used as a model drug, whereas a range of HPC polymers with varying M_w, kindly donated by Nisso Chemical Europe GmbH, were used for the preparation of solid dispersions: SSL (40 kDa), L (84 kDa), M (394 kDa). Dichloromethane (99.8 %, Sigma-Aldrich) and methanol (99.9 %, Carlo Erba) were used as solvents for spray drying. Acetonitrile (99.9 %, Carlo Erba) and trifluoracetic acid (99.9 %, Sigma-Aldrich) were used for mobile phase preparation for HPLC analysis. Hydrochloric acid (37 %, Fluka), NaCl (99 %, Sigma-Aldrich), KCl (99 %, Sigma-Aldrich), Na_2HCO_3 (99 %, Sigma-Aldrich), $CaCl_2$ (99 %, Sigma-Aldrich) were used for the preparation of the dissolution media.

As bile salts source we used porcine bile extract, purchased from Sigma-Aldrich. This extract contains 50 wt% bile acids, 6 wt% phosphatidylcholine, less than 0.06 wt% Ca^{2+} (Zangenberg, 2001), 1.8 wt% cholesterol, 4.3 wt% fatty acids (Vinarov, 2012). The composition of the bile salts in this extract is 13 wt% hyodeoxycholic acid, 18 wt% deoxycholic acid, 5 wt% cholic acid, 39 wt% glycodeoxycholic acid, and 24 wt% taurodeoxycholic acid (Vinarov, 2012). The percentages of these bile acids and the corresponding molecular masses were used to calculate an average molecular mass of 442 g/mol, which was used to define the average molar concentration of bile salts in the experiments.

For few of the model experiments, 3F powder from biorelevant.com, containing sodium taurocholate and lecithin was used in place of the porcine bile extract, in order to facilitate data interpretation. Solutions equivalent to 10 mM taurocholate and 2.5 mM lecithin were prepared to obtain 10 mM fed state simulated intestinal fluids (FeSSIF).

2.2. Spray-drying

GLB and HPC polymers were dissolved in a dichloromethane and methanol mixture (80:20 v/v) at 1:3 drug to polymer ratio and total solids concentration of 5 % (w/v), corresponding to 1.25 % (w/v) GLB and 3.75 % (w/v) polymer. The solution was then spray-dried on Buchi mini-B-290 spray drier. Spray drying was performed using the following parameters: inlet temperature: 50 °C; outlet temperature 35 °C; aspirator: 70 %; feed flow rate: 10 mL/min; rotameter gas flow (Q-flow): 30 mm, equal to a gas flow rate of 357 L/h with a pressure drop of 0.23 bar and actual volume flow (at standard temperature and pressure) of 439 L/h. Nitrogen with purity 99.99 % was used as a drying gas. Those spray-drying conditions were shown to give optimal yield of 50 to 70 %. The spray-dried powders were then placed under vacuum for 24 h at room temperature ($T = 23$ °C) to remove any residual solvent and afterwards were stored in a desiccator filled with silica gel at room temperature ($T = 23$ °C).

2.3. Solid-state analysis

The solid state of the spray-dried GLB and GLB-HPC powders, as well as the corresponding physical mixtures, was studied by polarized light microscopy (PLM), wide angle X-ray scattering (WAXS) and differential scanning calorimetry (DSC). The materials were studied after preparation (spray-drying or physical mixing), after storage for 4 months (stored at 22 °C in desiccator) and at the end of a dissolution experiment. The spray-dried powders, such as the pure GLB (SD-G), GLB-HPC SSL (SD-G-SSL) and GLB-HPC L (SD-G-L) did not require any specific sample preparation and were studied directly. The solid state of the spray dried particles that were collected at the end of a dissolution experiment was studied by the following protocol. The whole sample from the dissolution experiments was filtered through a 200 nm NY filter on a Buchner funnel, linked to a water jet vacuum pump. The solid residue left on the NY filter was collected, then dried at ambient temperature (22 °C) for 1 h and analysed via DSC and WAXS. Endothermic peaks due to water evaporation, suggesting incomplete drying, were not observed in the DSC thermograms. For PLM after dissolution, the aqueous phase which contained solid particles was collected with a pipette from the middle part of the vessel while shaking, ensuring the homogeneity of the aspirated sample, placed on microscope slide and observed under polarized light.

2.3.1. Polarized light microscopy

(A) Imaging of spray-dried powders

The optical observations were performed with AxioImager.M2m microscope (Zeiss, Germany) in transmitted, cross-polarized white light. A λ-compensator plate was placed after the studied specimen and before the polarizer at 45° angle with respect to both the analyser and polarizer, resulting in a characteristic magenta color of the background of the images. Long-focus objectives with magnifications 10×, 20×, 50 × were used for the observations.

(B) Imaging of undissolved amorphous GLB after gastric phase. SD-G (10 mg) was placed in 10 mL glass bottle. Simulated gastric fluid (10 mL) was then added. The suspension was homogenized on vortex for 30 min at 37 °C. Afterwards, two drops of the suspension were placed on microscope slide; the sample was then covered with cover slide on top and the GLB particles were observed under polarized light.

(C) Determination of the onset of crystallization. Amorphous GLB (SD-G) was placed on a microscope slide. Two drops of simulated gastric fluid were placed over the powder. The composition and the preparation protocol for the simulated gastric fluid are described in section 2.4. The sample was then covered with cover slide on top and the crystallization process was observed under polarized light, as a function of time. As dissolution experiments at gastric conditions have shown that drug dissolution is minimal (below LOD), the precise concentration of solids in the gastric in situ imaging experiment does not play a role in the observed processes, which relate to the solid state of the particles, and not to their dissolution (all particles remain undissolved).

(D) Dissolution-crystallization observations of amorphous GLB. Minimal amount of SD-G particles (less than 0.1 mg) were placed in a petri dish on top of aluminum thermostatic chamber with several cut-out optical windows. The temperature in the metal chamber was set to 37 °C and was controlled using a cryo-thermostat JULABO CF30. A calibrated thermocouple probe (with an accuracy of ± 0.2 °C, calibrated by a precise mercury thermometer in the relevant temperature range) was placed in an adjacent orifice to measure the temperature in the petri dish. Dissolution and crystallization was imaged by adding to the petri dish 2 mL of simulated intestinal fluid consisting of 10 mM sodium taurocholate + 2.5 mM lecithin solution (10 mM FaSSIF) to SD-G. Phosphate buffer (10 mM NaOH, 100 mM NaCl, 28.6 mM NaH_2PO_4) was used to keep constant pH = 6.5. By performing the experiment in the described way (minimal amount of SD-G solids in 2 mL fluids) we

aimed to ensure sink conditions, allowing us to observe the dissolution of the particles.

In a separate set of experiments, dissolution and crystallization was imaged in pure buffer solutions. Two drops of phosphate buffer (pH 6.5) or 120 mM bicarbonate buffer (pH 9.5) were added to minimal amount of SD-G solids (less than 0.1 mg) placed on microscope slide, and a cover slide was placed on top. The dissolution and crystallization processes were monitored as a function of time under polarized light. Sink conditions were maintained at the higher pH (9.5), as demonstrated by the quick and complete dissolution of all SD-G solids, whereas rapid crystallization prevented dissolution at the lower pH (6.5). The pH values were selected in order to mimic the intestinal conditions (pH = 6.5), allowing us to disentangle the effects of pH and bile salts on dissolution and crystallization of the amorphous solids, whereas the higher pH = 9.5 was selected to be sufficiently above the pKa of the weak acid GLB (pKa = 5.6), in order to illustrate the impact of ionization on dissolution rate and crystallization.

2.3.2. Wide angle X-ray scattering

WAXS measurements were carried out with XEUSS 3.0 SAXS/WAXS System (Xenocs, Sassenage, France) with a CuKα X-ray source (λ = 0.154 nm, Xeuss 3.0 UHR Dual source Mo/Cu, Xenocs, Sassenage, France) and Eiger2 4 M detector (Dectris Ltd., Baden Deattwil, Switzerland) with slit collimation. The apparatus was operated at 50 kV and 0.6 mA with sample to detector distance of 300 mm to access a q-range of 0.03–1.5 $Å^{-1}$. Data acquisition time was 20 min. The solid-state detector acquires a 2D image, in which all scattering vectors (angles) in the described range correspond to respective pixels of the detector image. The exposure time was thus the same for all angles studied, as the scattering data was obtained simultaneously for all angles.

Samples were enclosed into 2.5 mm in diameter metal O-rings covered with two Kapton windows with 12.5 μm thickness.

The scattered intensity was normalized to the incident intensity and was corrected for the background scattering from the empty sample holder. Calibration to absolute scale was used. The measurements were performed at ambient temperature of ca. 20 °C.

2.3.3. Differential scanning calorimetry

DSC measurements were performed using DSC Discovery 250 TA Instruments, USA. Each sample was weighed accurately and hermetically sealed in an aluminium DSC pan, then placed on one of the thermocouples in the measurement chamber of the instrument. An empty reference pan was placed on the second thermocouple. The samples were then heated from 30 °C to 190 °C with 10 °C/min temperature ramp, while measuring the normalized heat flow as W/g.

2.4. Biorelevant dissolution assay

The dissolution of GLB (crystalline and amorphous) and the spray-dried formulations was studied by a modified bicarbonate-based two-stage *in vitro* gastrointestinal tract model (Vinarov, 2012), which begins with a gastric stage (30 min), followed by a switch to intestinal conditions via the addition of bicarbonate and bile salts and 120 min shaking to monitor intestinal dissolution.

The experiments were performed in 10 mL glass bottles and shaking on Eppendorf ThermoMixer C at 400 rpm at T = 37 °C was used for homogenization. Gastric conditions were mimicked by mixing 2.16 mL 0.25 M HCl and 2.83 mL saline solution (59 mM NaCl, 35 mM KCl, 3.5 mM $CaCl_2$), yielding final volume of the gastric fluids of 5 mL and pH = 1.3. Gastric fluids with the same composition were used also for the in situ imaging experiments. After 30 min of shaking of the gastric fluids, 1.66 mL of 720 mM bicarbonate buffer, 1.66 mL 2.5 % bile extract and 1.66 mL water were added (total volume of 5 mL). Hence, a 1:1 dilution ratio was used for the gastrointestinal transfer step. The final concentrations of all components in the intestinal fluids were: 1.25 % porcine bile extract (corresponding to 10 mM bile salts), 120 mM sodium bicarbonate, 54 Mm HCl, 16.8 mM NaCl, 10 mM KCl, 1 mM $CaCl_2$ with pH increasing from 6.5 from the moment of mixing the gastric and the intestinal phase to 6.8 at the end of the experiment (after 120 min), due to the continuous release of CO_2. Samples for analysis were taken after 10, 30, 60, 90 and 120 min with a thermostated syringe and were filtered using 200 nm NY filter, diluted with methanol (1:4) and analyzed by high-performance liquid chromatography (HPLC). Formulations were introduced either in the gastric phase, or directly at intestinal conditions.

2.5. HPLC analysis

The analysis was carried out on Shimadzu apparatus, equipped with two high-pressure mixing binary gradient pumps (LC-20AD), autosampler (SIL-10ADvp) and a dual wavelength UV–VIS detector (SPD-10Avp) operating at 230 nm. The column of choice was Waters X-bridge (150 mm × 4.6 mm, 3.5 μm particle size with column guard VanGard (Waters), 3.9 mm × 5 mm – C18, 3.5 μm) at 40 °C. Isocratic elution mode was used, with the eluent flow rate set to 1 mL/min, A-ACN 60 % B-0,1 % TFA 40 %. Injection volume was set to 20 μL.

GLB calibration curve was made by preparing a stock solution of the drug in a methanol–water mixture (4:1) with a concentration of 100 μg/mL. Six standard solutions, obtained by diluting the stock solution, were analysed to generate a calibration curve in the range of 1 to 100 μg/mL, with a limit of quantification LOQ = 0.1 μg/mL.

2.6. Dynamic light scattering (DLS)

Samples from the gastrointestinal tract model were taken after 60 min of the intestinal stage using a thermostated syringe. The samples were then filtered with 200 nm NY filter. The size of colloidal aggregates was studied using a variable multi-angle light scattering instrument (LS spectrometer, LS instruments AG, Switzerland). The measurements were taken at 37 °C at a scattering angle of 90°.

3. Experimental results

The following sections are presented below: characterization of spray-dried materials (section 3.1), drug dissolution of spray-dried materials in biorelevant media (section 3.2) and in-situ studies of dissolution and crystallization (section 3.3).

3.1. Characterization of spray-dried materials

Three samples of amorphous solid materials were obtained by spray-drying: (1) SD-G, (2) SD-G-SSL and (3) SD-G-L. The high viscosity of the organic solvent solution of the polymer with the highest M_w (HPC-M) prevented spray-drying of such formulation. The solid-state properties of these materials were monitored by using PLM, WAXS and DSC.

The reference crystalline GLB was characterized by well-defined crystals that exhibited birefringence under polarized light (Fig. 1A). In contrast, pure GLB (in absence of any polymer) was composed of irregularly shaped particles with no apparent birefringence, indicating it was in the amorphous state (Fig. 1B). The spray-dried formulations containing GLB + polymer (SD-G-SSL and SD-G-L) showed similar behaviour, characterized with the lack of birefringence (Figure S1 in the Supporting information).

To further investigate the solid-state properties of the spray-dried materials, WAXS measurements were performed. Bragg peaks indicating crystalline structure were observed at for the reference crystalline GLB (Fig. 2) and for the physical mixtures of crystalline GLB with the studied polymers (Figure S2 in the Supporting information). The observed Bragg peaks corresponded to the type I polymorph of GLB (Table S1 in the Supporting information) (Panagopoulou-Kaplani and Malamataris, 2000). The WAXS measurements of the spray dried powders showed a characteristic amorphous halo and no Bragg peaks for the

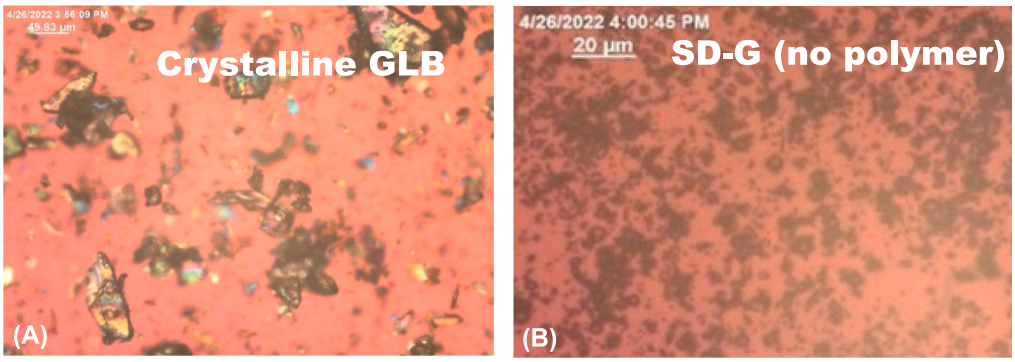

Fig. 1. PLM images of (A) crystalline and (B) spray-dried GLB.

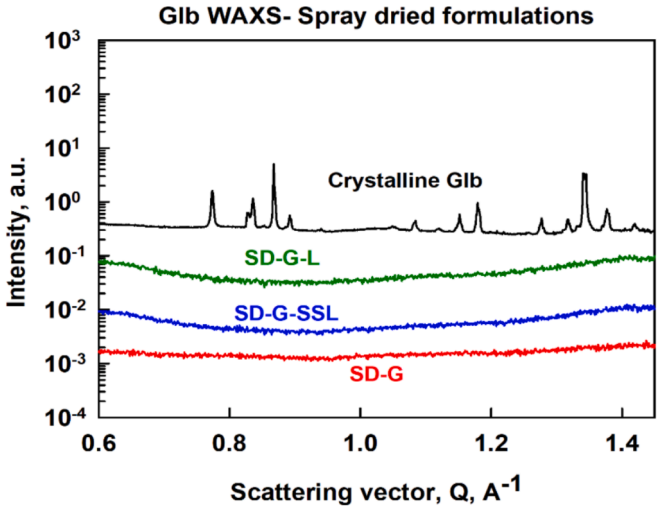

Fig. 2. WAXS analysis of the studied materials: crystalline GLB (black), SD-G-L (green), SD-G-SSL (blue) and SD-G (red). (For interpretation of the references to color in this figure legend, the reader is referred to the web version of this article.)

spray-dried materials (Fig. 2), which confirmed their amorphous nature that was suggested by PLM.

In addition to the PLM and WAXS measurements, thermal analysis by DSC was also performed on spray-dried materials and physical mixtures to investigate their solid-state properties. The melting point of the reference crystalline GLB was observed at 175 °C, corresponding to GLB type I polymorphic form, which has a characteristic melting point of 172–175 °C (Panagopoulou-Kaplani and Malamataris, 2000; Suleiman and Najib, 1989; Sanz, 2012). Melting peak was not observed in the thermograms of the spray-dried materials (Fig. 3), which corroborates the amorphous state of GLB that was established by PLM and WAXS. Evidence of a glass-transition temperature could be observed for the SD-G ($T_g = 70$ °C) and GLB + HPC SSL ($T_g = 50$ °C), which was not detected for GLB + HPC L.

The melting of the crystalline compound could be detected in physical mixtures (Figure S3 in the Supporting information), however, the melting point was shifted to slightly lower temperature (168 °C) which may be due to the melting of the polymers that can then act as plasticizers. Glass transitions were not observed in the physical mixtures.

The stability of the formulations was monitored with DSC measurements for 4 months (Fig. 3B). The thermograms showed no signs of crystallization for the systems which contained polymer after 4 months. The pure amorphous GLB showed signs of changes in the solid-state characteristics. Exothermic crystallization peak appeared at 150 °C with enthalpy 60.6 J/g, followed by endothermic melting peak at 172 °C with enthalpy 68.4 J/g, suggesting the crystallization of the type I GLB polymorph (Sanz, 2012).

3.2. Drug dissolution of spray-dried materials in biorelevant media

Drug dissolution from neat amorphous GLB and from formulations stabilized by HPC SSL and HPC L was studied at two conditions. In the first set of experiments, the materials were introduced directly at the intestinal stage of the in vitro model, mimicking the scenario in which the spray-dried powder is administered by a gastro-resistant capsule. In

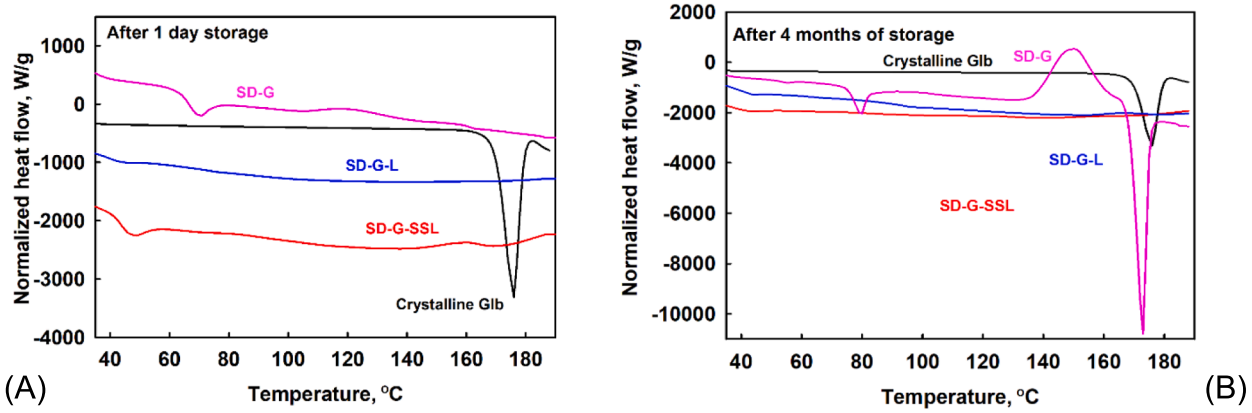

Fig. 3. DSC thermograms during heating of spray-dried formulations after storage for (A) 1 day or (B) four months at $T = 22$ °C in desiccator: SD-G (pink), SD-G-L (blue) and SD-G-SSL (red). The thermogram of crystalline GLB (black) is displayed for the purpose of comparison. (For interpretation of the references to color in this figure legend, the reader is referred to the web version of this article.)

the second set of experiments, the drug was introduced in the gastric phase, followed by a switch to intestinal conditions.

The first series of drug dissolution measurements were performed by introducing the spray-dried formulations directly at intestinal conditions Fig. 4A.

All amorphous materials showed significantly better dissolution performance (concentrations between 100 and 300 μg/mL), compared to the reference crystalline drug (≈ 1 μg/mL), see Fig. 4A. The presence of polymers *per se* did not have a large impact on the aqueous solubility of crystalline GLB, as determined by dissolution experiments with physical mixtures of crystalline GLB and polymers (Figure S4 in the Supporting information) and by 24 h shake-flask equilibrium solubility experiments (GLB solubility of 1.0 ± 0.1, 1.0 ± 0.3 and 2.1 ± 0.7 μg/mL for HPC M, L and SSL, respectively). The formulations containing HPC SSL and HPC L polymers showed similar performance, releasing ≈ 100 μg/mL GLB after 5 min at intestinal conditions, which increased gradually to ≈ 300 μg/mL after 120 min (Fig. 4A). In contrast, drug dissolution from the neat amorphous material reached only to 160 μg/mL after 120 min.

To check the impact of gastric conditions on drug dissolution, experiments were performed in a gastrointestinal tract transfer model, where the pure drug or spray-dried formulation was introduced first in the gastric phase, which after 30 min was switched to intestinal conditions by the addition of bicarbonate and bile salts Fig. 4B. GLB concentrations were measured only in the intestinal phase of the model, as experiments with pre-dissolved polymers showed that the aqueous GLB in the gastric phase was below the detection limit of the analytical method.

After exposure to gastric conditions, the HPC SSL formulation showed the best performance, followed by HPC L, whereas SD-G and the crystalline drug led to very low drug concentrations (Fig. 4B). However, the measured intestinal GLB concentrations after exposure to gastric conditions were generally lower (up to ≈ 200 μg/mL, Fig. 4B), compared to when the formulations were administered directly in the intestinal fluids (up to ≈ 300 μg/mL, Fig. 4A).

Comparing the introduction of SD-G to the gastric or intestinal phase, a significant change in the behaviour was observed: the exposure to gastric conditions caused a large decrease in the aqueous GLB concentrations (10 μg/mL after 120 min), in contrast to the high concentrations measured when the amorphous drug was directly introduced in the intestinal phase (160 μg/mL after 120 min). Hence, gastric conditions were found to have a significant impact on amorphous GLB dissolution.

3.3. Model experiments

3.3.1. Gastric conditions: Effect of polymer on the amorphous to crystalline transition

To gain more information about the mechanisms that drive the large shift in the dissolution profile of amorphous GLB depending on its exposure to gastric conditions, additional experiments were performed. The impact of polymers on dissolution and solid state of SD-G was tested at two conditions that corresponded to the dissolution studies of the spray-dried materials: (1) introduced at gastric conditions then switched to intestinal conditions and (2) introduced directly at intestinal conditions (no gastric phase). For all experiments described in this section, neat amorphous GLB was used, whereas the polymers were pre-dissolved in either the gastric or the intestinal fluids.

HPC SSL, L and M polymers were pre-dissolved at gastric conditions to match the polymer concentration in the experiments with spray-dried materials (6 mg/mL in the gastric phase, before dilution to 3 mg/mL at intestinal conditions) and SD-G was added. A sample in the absence of any pre-dissolved polymer was also prepared. Solid-state analysis of the undissolved GLB solids was performed by DSC and WAXS at the end of the gastric phase. Drug dissolution was monitored during the gastric and intestinal phase.

For all studied systems, gastric concentrations of GLB were below the limit of detection (Fig. 5). However, significant differences were observed in the intestinal phase: highest GLB concentrations (up to ≈ 160 μg/mL GLB) were measured in presence of HPC SSL, followed by HPC L (≈ 100 μg/mL GLB) and HPC M (≈ 60 μg/mL).

To confirm the role of the gastric phase in GLB crystallization, solid-state analysis of undissolved solids collected at the end of the gastric phase was performed. In the absence of polymer, DSC analysis showed a melting peak at $T = 153$ °C, demonstrating a transition from amorphous state to crystalline form, most probably as type III polymorph (Hassan, 1997) (Fig. 6A). Such peak was not detected when HPC SSL or HPC L were pre-dissolved in the media. HPC M was less efficient in stabilizing the amorphous GLB, as evidenced by the exothermic crystallization peak at $T = 130$ °C, followed by an endothermic melting peak at $T = 172$ °C (characteristic for the initial crystalline GLB polymorph).

The accompanying results from the WAXS measurements of the undissolved solids that were collected at the end of the gastric stage ($t = 30$ min) in absence of polymer showed multiple peaks at low q range (between 0.6 and 1.6 A^{-1}), indicating transition from amorphous to crystalline state (Fig. 6B). The presence of HPC SSL in the gastric medium prevented crystallization, as illustrated by the lack of scattering peaks. The diffractograms of amorphous GLB in presence of HPC L or HPC M

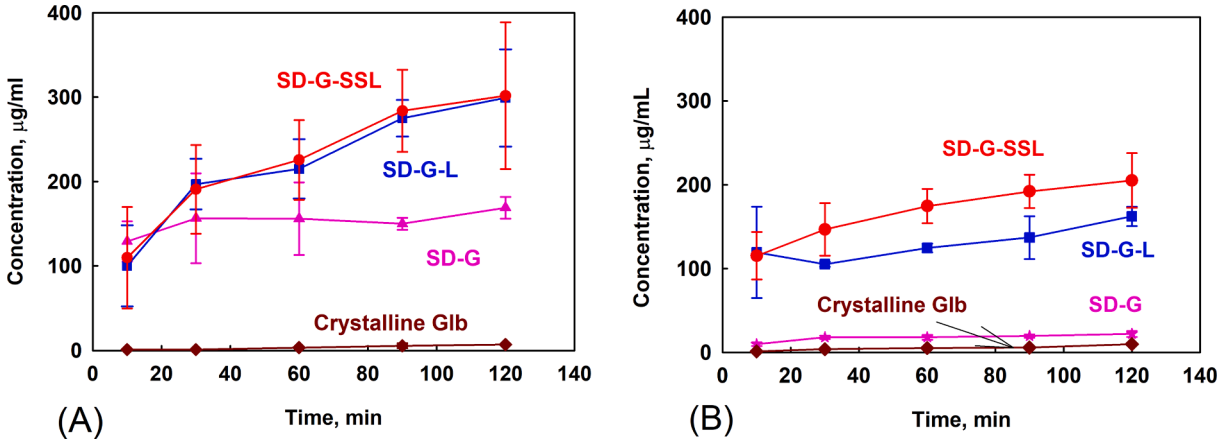

Fig. 4. Dissolution profile of spray-dried amorphous GLB formulations introduced (A) directly into the intestinal phase of the biorelevant dissolution media and (B) in the stomach phase, which was then switched to intestinal conditions. SD-G-SSL, red circles, SD-G-L, blue squares and SD-G, pink stars. The dissolution of crystalline GLB (brown diamonds) is displayed for the purpose of comparison. The presented results are averaged from at least 3 independent samples (n ≥ 3). Error bars can be smaller than the symbols. (For interpretation of the references to color in this figure legend, the reader is referred to the web version of this article.)

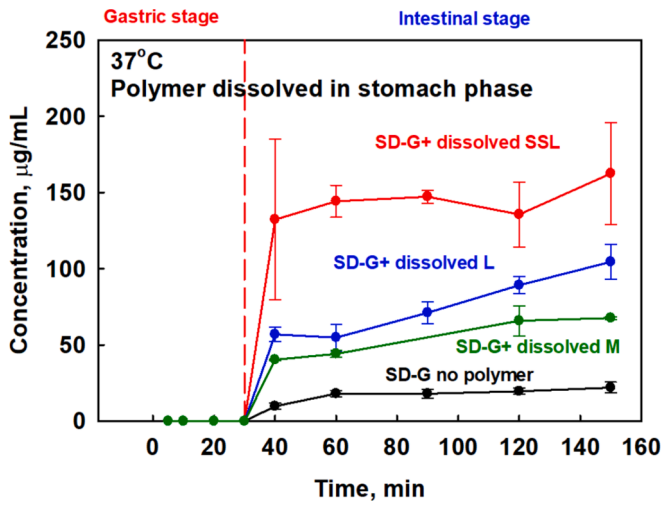

Fig. 5. Dissolution profile of amorphous GLB introduced at gastric conditions in presence of pre-dissolved HPC SSL (red circles), HPC L (blue squares), HPC M (green triangles) and in absence of any pre-dissolved polymer (pink stars). Results are averaged from three independent experiments. (For interpretation of the references to color in this figure legend, the reader is referred to the web version of this article.)

showed 2 groups of minor peaks at $0.8A^{-1}$ and $1.3A^{-1}$, (showed with arrows) indicating partial GLB crystallization. Different GLB diffraction pattern was observed when the drug has been exposed to gastric fluids compared to the reference crystalline compound, with additional peaks emerging at approximately 0.35 and 0.6 A^{-1}, while the two sets of peaks around 0.8 and 1.3 A^{-1} underwent changes in terms of peak ratios and appearance. The difference in the diffraction patterns and melting temperature suggests the formation of different GLB polymorph.

The results presented above showed that amorphous GLB crystallizes when placed in contact with gastric solution, unless polymers have been pre-dissolved in this medium, in which case crystallization is inhibited. To gain further insight on the mechanisms and interplay between dissolution, crystallization and its inhibition, amorphous GLB particles were imaged by PLM after contact with biorelevant media, in presence or absence of polymers. The appearance of birefringence in the particles was used to identify the onset of crystallization. Two types of experiments were performed, which were aimed either at capturing rapid processes (timeframe of seconds or minutes), or at imaging the solid particles at the end of the gastric stage of dissolution.

In the first experiment, amorphous GLB particles (no polymer) were placed on a glass slide, a droplet of gastric media was added on top, and images were immediately collected. This was done in order to observe the fast processes related to the transition of the amorphous GLB particles to a crystalline state. Birefringence, indicating crystallization, was observed after 1 min (Fig. 7). Careful analysis of the amorphous-to-crystalline transition of the aggregated particles showed that crystallization starts from particles found at the outer edges of the aggregate, rather than the centrally-located particles. Afterwards, the crystallinity spreads from these initial crystal seeds, reaching the central parts of the aggregate.

In the second series of experiments, neat amorphous GLB was placed in gastric fluids with or without pre-dissolved polymer, the sample was shaken for 30 min at $T = 37$°C, replicating the conditions of the dissolution experiment, and afterwards samples were taken for PLM. This was done in order to gain insight on the solid state of the drug at the end of the gastric stage. The results showed extensive aggregation and birefringence when the amorphous GLB was placed in the gastric phase (Fig. 8).

In agreement with the results from the *in-situ* experiment (Fig. 7), crystallization was observed for single drug particles and for particles found on the outer edges of the large aggregates. In contrast, very limited particle aggregation and no birefringence was observed when HPC SSL was pre-dissolved in the gastric phase. The presence of HPC L or M inhibited GLB particle aggregation to a lesser extent (compared to HPC SSL) and birefringence could be observed in several GLB particles, illustrating the weaker crystallization-inhibition effect of the higher-M_w HPC polymers.

The results described so far can account for the low aqueous GLB concentrations measured at gastric conditions, when polymers are not present to inhibit the amorphous-to-crystalline transition. However, it remains unclear why aqueous GLB concentrations remain very low at gastric conditions, even in the cases where HPC was present and the drug remained amorphous. This contrasts with intestinal conditions, where very high aqueous GLB concentrations were measured for the amorphous solids. To check the hypothesis that wetting and solubilization effects may play a role (no surface-active compounds in the gastric phase vs. bile salts and phospholipids in the intestinal phase), a dedicated experiment was performed: amorphous GLB particles were added to gastric media with pre-dissolved surfactant (1 % sodium dodecyl sulphate, SDS) and crystallization inhibitor (6 mg/mL HPC SSL, replicating the polymer concentration in the gastric fluids of a standard

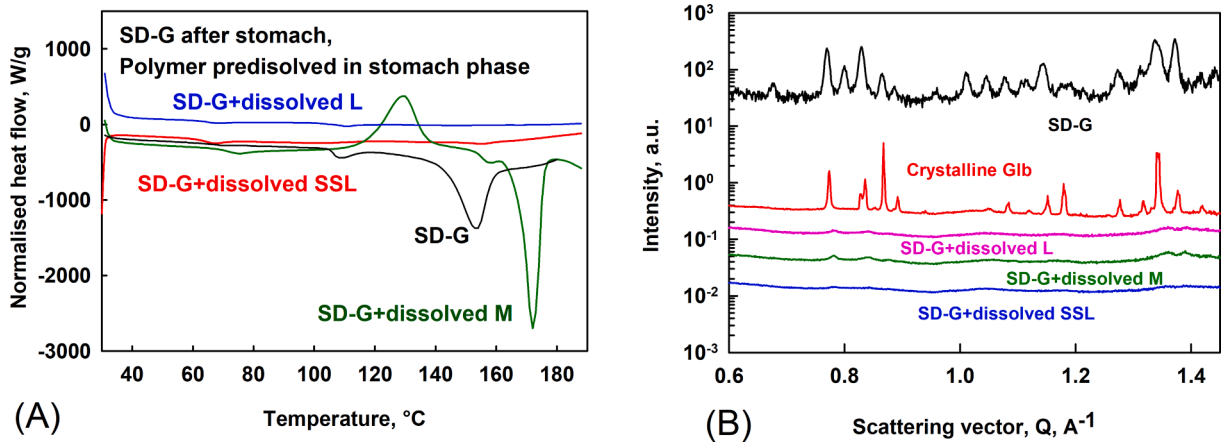

Fig. 6. (A) DSC thermograms of undissolved solids recovered after being exposed for 30 min to gastric conditions: SD-G (black line), physical mixture of GLB + HPC SSL (red line), physical mixture of GLB + HPC L (blue line), physical mixture of GLB + HPC M (green line). (B) WAXS data of undissolved amorphous GLB solids recovered after being exposed for 30 min to gastric conditions in presence of pre-dissolved HPC M (pink line), HPC L (green line), HPC SSL (blue line) or without pre-dissolved polymer (black line). WAXS data of crystalline GLB (red line) is shown for the purpose of comparison. (For interpretation of the references to color in this figure legend, the reader is referred to the web version of this article.)

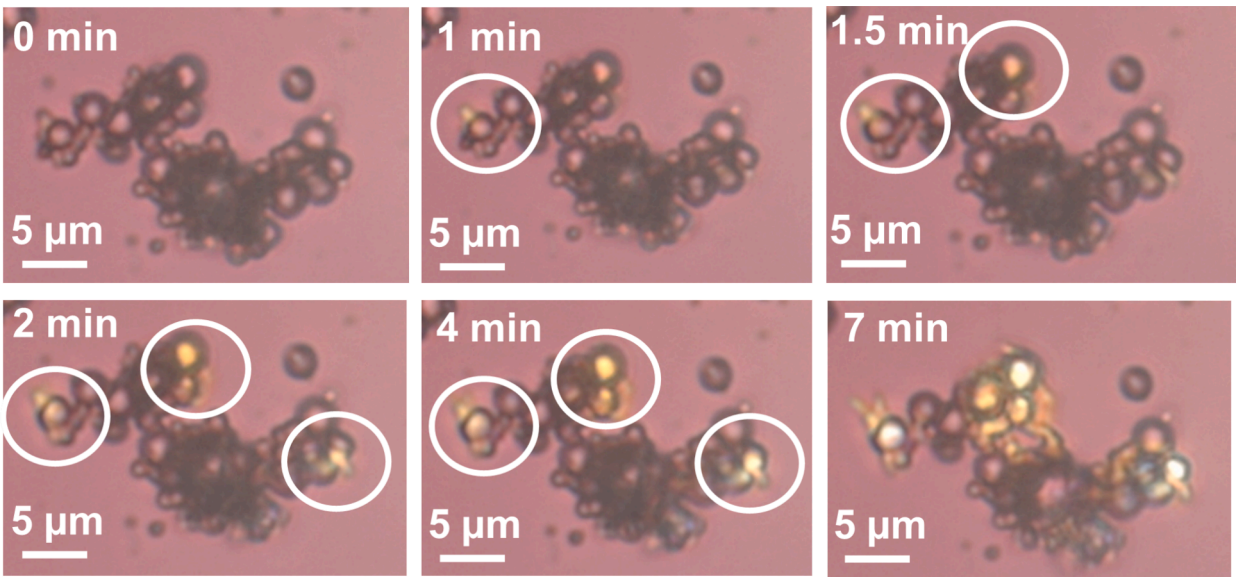

Fig. 7. PLM images of amorphous GLB particles in gastric media as a function of time (no polymer).

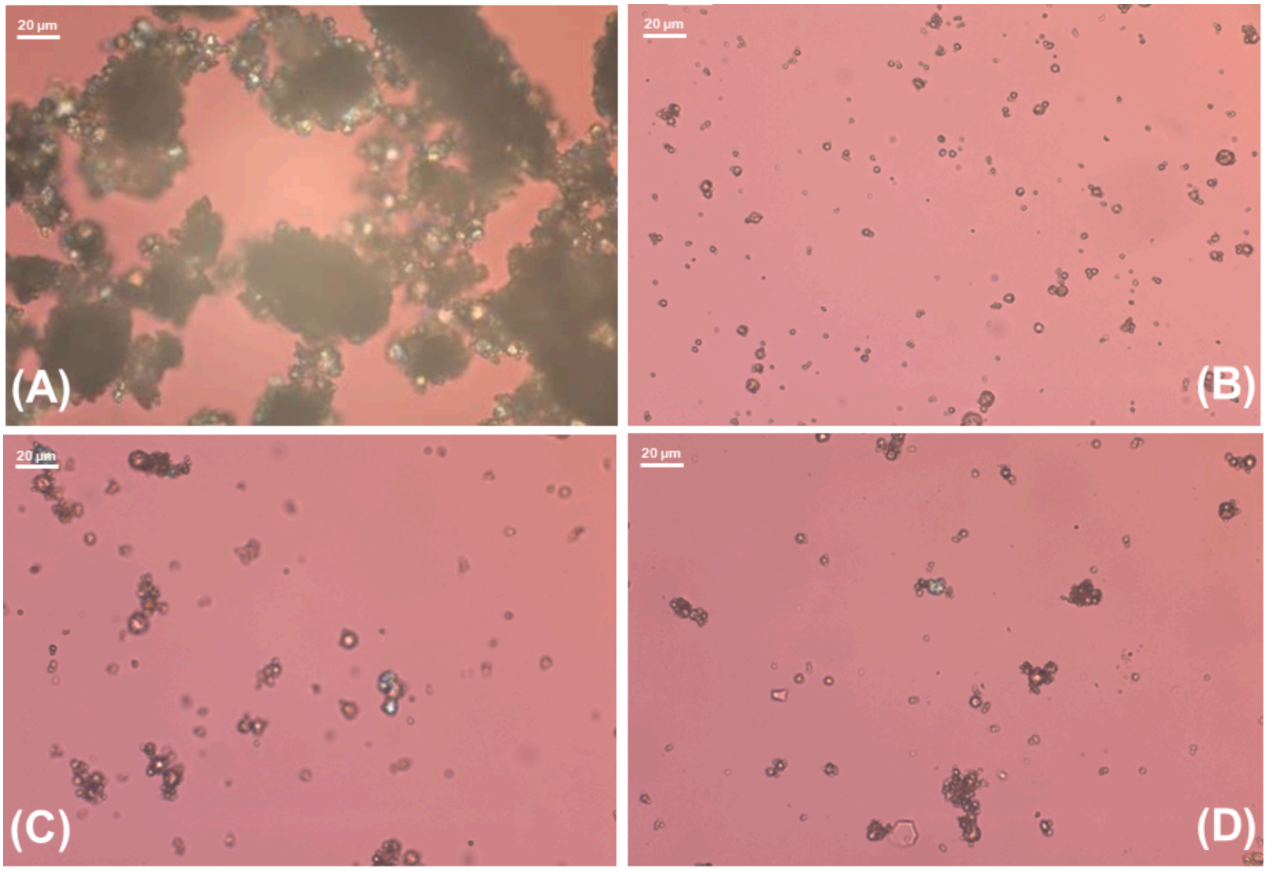

Fig. 8. PLM images of undissolved SD-G after 30 min in (A) gastric fluids, (B) 6 mg/ml HPC SSL in gastric fluids, (C) 6 mg/ml HPC L in gastric fluids, (D) 6 mg/ml HPC M in gastric fluids.

dissolution experiment). Control experiment with crystalline GLB was also performed.

At the end of the gastric phase (t = 30 min), much higher aqueous GLB concentrations were measured for the amorphous GLB, compared to the crystalline material: 81 vs. 21 µg/mL, respectively. Unpublished results from our lab show that a similar concentration of SDS (1.14 %) at pH = 3 (at which GLB is still neutral) solubilizes crystalline GLB and increases the apparent solubility to 64 µg/mL, compared to 0.18 ± 0.09 ng/mL in buffer (measured by LC-MS/MS). This further emphasizes the role of solubilization in increasing the aqueous GLB concentrations *per se*. Interestingly, DSC analysis showed that the surfactant caused crystallization of GLB, as evidenced by a clear melting peak at $T = 160$ °C. Hence, even at the low pH of gastric conditions, improved wetting and solubilization significantly increased the aqueous GLB concentrations,

while competing with crystallization.

3.3.2. Intestinal conditions: Effect of bile and polymer on amorphous to crystalline transition

The results described above clearly showed that the exposure of amorphous GLB to gastric conditions in absence of polymer causes drug crystallization. It this context, it was interesting to investigate the stability of amorphous GLB at intestinal conditions, without prior exposure to gastric conditions.

For this purpose, the SD-G was introduced in four types of intestinal dissolution media: (1) blank media, composed of buffers and salts (pH = 6.5 – 7.0), (2) standard intestinal media, containing porcine bile extract, (3) blank media with pre-dissolved 3 mg/mL HPC SSL and (4) intestinal media + pre-dissolved 3 mg/mL HPC SSL. The polymer concentration was selected in order to replicate the concentration of polymer at the intestinal stage of the dissolution experiments. The undissolved residue at the end of the experiment was collected for DSC analysis.

When introduced into the blank media, very low aqueous GLB concentrations were measured (2–3 μg/mL), indicating drug crystallization (Fig. 9A). In contrast, supersaturated GLB concentrations were measured in the other three media. In presence of both bile extract and HPC SSL, aqueous GLB was consistently higher than in presence of only bile extract. The presence of HPC SSL yielded slightly lower (on average) GLB concentrations compared to the bile extract.

Solid-state analysis by DSC at the end of the intestinal phase showed no signs of crystallization when HPC SSL is present in the media in combination with bile extract (Fig. 9B). In contrast, a peak characteristic for the melting of crystalline GLB, T = 172 °C, was observed for the control (amorphous GLB in buffer). A wider melting peak around T = 164 °C was determined in presence of bile extract, which may be due to a plasticising effect of bile components on GLB crystals. In presence of HPC SSL, a very wide and shallow peak at T = 150 °C was observed, indicating the stronger plasticising effect of the polymer, or the melting of the type III polymorph.

Interestingly, higher aqueous GLB concentrations were measured for the bile-only sample, where a substantial melting peak of crystalline GLB was observed, compared to the HPC-SSL-only sample, where a very small melting peak at lower temperature was correlated with lower aqueous drug concentrations. Most likely, this is due to a competition between dissolution and crystallization, as in both cases the percentage of dissolved drug is small (ca. 15 %): bile salts offer better wetting and penetration of the aqueous phase in the amorphous material, which allows quicker drug dissolution before surface crystallization occurs.

Similarly to the previous section, in-situ studies of amorphous solids dissolution and crystallization were performed by PLM. To facilitate the interpretation of the images, simulated intestinal fluids (3F powder, biorelevant.com) at a taurocholate concentration of 10 mM and lecithin concentration of 2.5 mM at pH = 6.5 were used to study amorphous GLB dissolution (Fuchs, 2015).

The obtained images showed a very quick dissolution of the

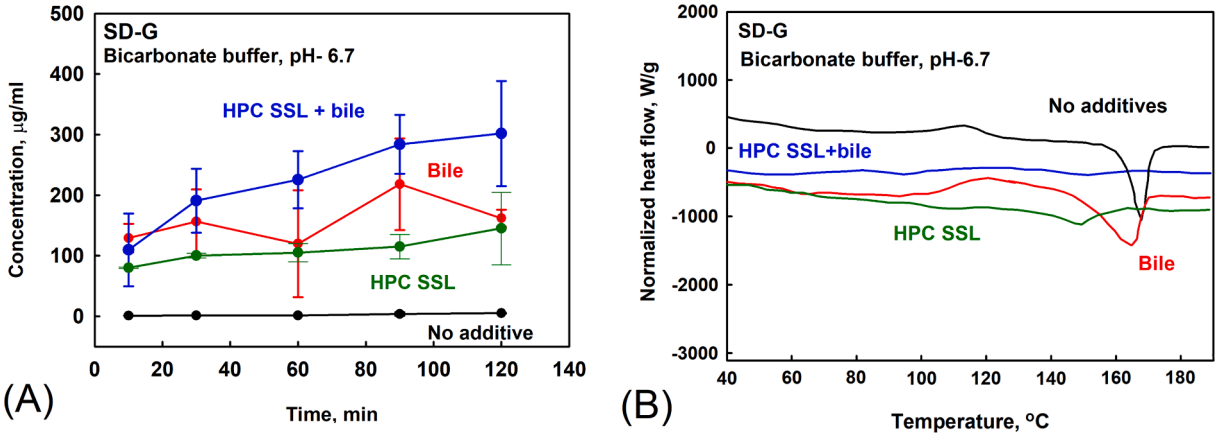

Fig. 9. (A) Aqueous GLB concentrations as a function of time and (B) DSC thermograms of the undissolved residue, obtained after amorphous GLB is added in porcine bile extract + 3 mg/mL HPC SSL (blue), porcine bile extract (red), blank media with pre-dissolved 3 mg/mL HPC SSL (green) or blank media containing only intestinal salts and buffers (black). (For interpretation of the references to color in this figure legend, the reader is referred to the web version of this article.)

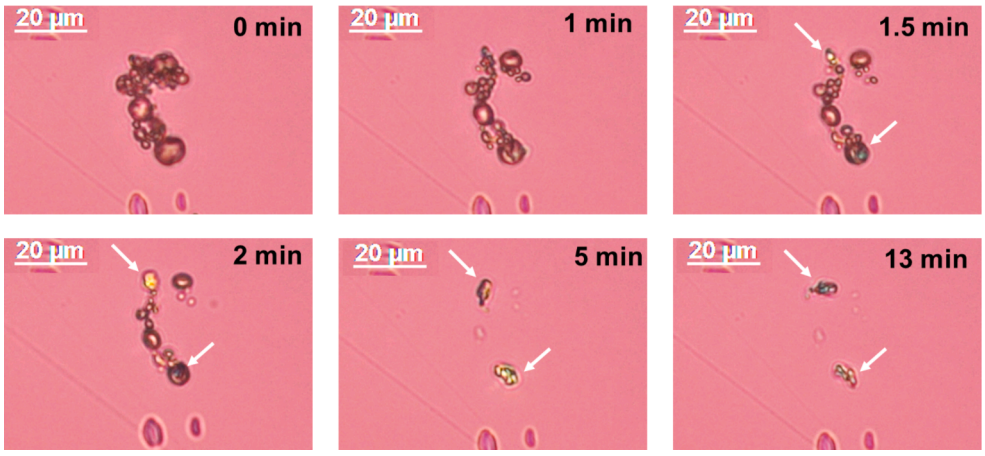

Fig. 10. PLM images of the dissolution of SD-G particles in 10 mM FaSSIF (10 mM sodium taurocholate, 2.5 mM lecithin) at pH = 6.5. The competition between dissolution and crystallization is clearly illustrated (white arrows indicate crystallized domains).

amorphous GLB particles (note that particles were composed only of GLB, no polymers), which competed with crystallization (Fig. 10). A significant decrease in the size of the particles was observed 1 min after contact with intestinal media, demonstrating very fast dissolution. However, crystallization also occurred very quickly, becoming apparent after 1.5 min. The crystallized particles were found on the edges of the particle aggregate, in agreement with the results presented in the previous subsection. Interestingly, crystallinity did not spread to the adjacent amorphous particles, although they were in contact with the GLB crystals. After 5 min, all amorphous particles had completely dissolved, while the GLB crystals remained undissolved for up to 13 min, without any changes in their size. The latter indicated that crystalline solubility was reached, and crystal growth was inhibited (at least at the studied short time scale).

Control experiment in which amorphous GLB solids were placed in contact with a buffer solution at the same pH = 6.5 were also performed (Fig. 11). Crystallization occurred at a similar timescale (1–2 min) but was much more pronounced, leading to amorphous-to-crystalline transition in more particles, compared to the experiments in presence of 10 mM sodium taurocholate and 2.5 mM lecithin. In the same time, dissolution was much slower and difficult to observe. Most likely, the micelles in the simulated intestinal fluids accelerate amorphous GLB dissolution by a combined effect of improved penetration of the aqueous media inside the particles (wetting effect) and micellar solubilization. Bile salts can also act as crystallization inhibitors, as shown in Fig. 10.

To substantiate the claim for the role of wetting in the dissolution of amorphous GLB in biorelevant media, the contact angles between GLB and a phosphate buffer solution (pH = 6.5), 10 mM FaSSIF (in the same buffer) or 3 mg/mL HPC SSL (in the same buffer) were measured (see Supporting information for the methodology). The pure buffer did not wet the GLB powder, indicating poor wetting and contact angle $\gg 90^{\circ}$. Literature data obtained by the sessile drop method confirmed that the contact angle of water on a GLB substrate is high, 131° (Sterren, 2021). In contrast, both 10 mM FaSSIF and 3 mg/mL HPC SSL significantly improved the wetting, decreasing the contact angle to 62-66° and 85-88°, respectively.

To further illustrate the effect of pH on the dissolution of the amorphous GLB solids, in situ dissolution experiments were performed at higher pH of 9.5 with bicarbonate buffer and pure amorphous GLB without any polymer. Amorphous GLB dissolution was extremely quick, with the majority of solids dissolving in seconds (Movie 1 in Supporting information). Amorphous-to-crystalline transition was observed rarely, and the crystallized particles did not dissolve in contrast to the amorphous material (Fig. 12), similarly to the results in presence of FeSSIF at lower pH = 6.5 (Fig. 10).

3.3.3. Nanoaggregate characterization

In order to check for liquid–liquid phase separation and the

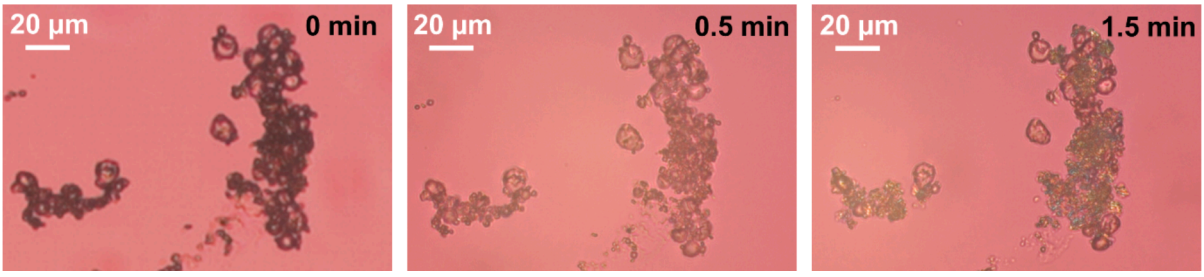

Fig. 11. PLM images of the dissolution of SD-G particles in phosphate buffer at pH = 6.5. Particle hydration and amorphous-to-crystalline transition occurred very quickly (after 1.5 min), whereas dissolution was not observed.

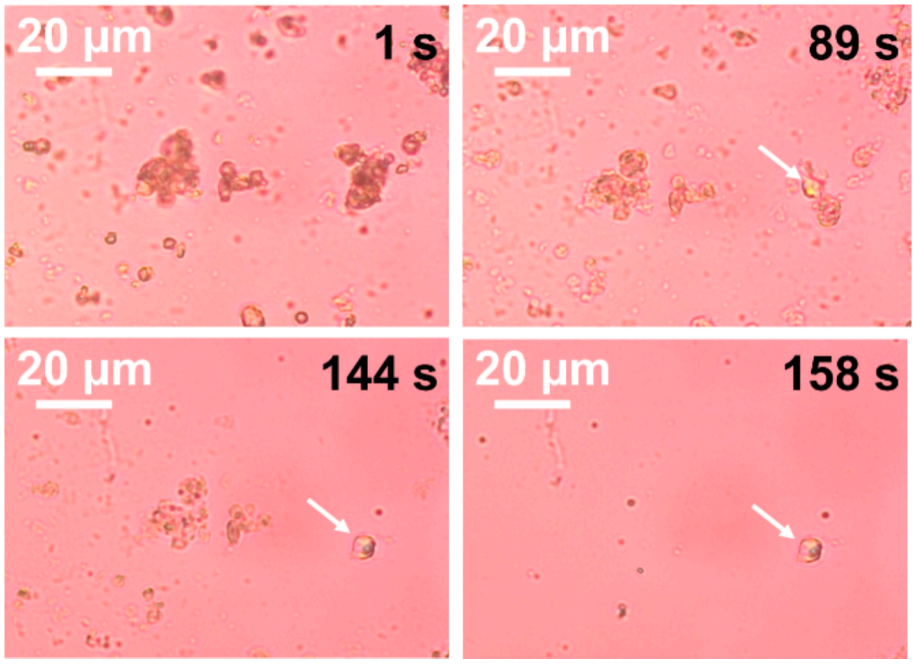

Fig. 12. PLM images of the dissolution of SD-G particles in 120 mM bicarbonate buffer at pH = 9.5. Very quick dissolution of all amorphous particle was observed, with one crystallized particle remaining undissolved (white arrows).

formation of drug-rich nanoparticles during ASD dissolution, we characterized by DLS the sample for which the highest aqueous drug concentrations were measured, GLB + HPC SSL. Samples were collected 60 min after GLB + HPC SSL dissolution at intestinal conditions.

In the porcine bile and bicarbonate-based media, an average aggregate diameter of ca. 100 nm with relatively high polydispersity was determined for both the reference blank intestinal media sample and the GLB + HPC SSL formulation (Figure S5 in the Supporting information). Images from cryo-TEM (see Supporting information for the methodology) confirmed the similar size of the aggregates in the two samples and the significant polydispersity (Figure S6 in the Supporting information).

Since the aggregate size in the intestinal media was relatively big and could potentially mask smaller or similar-sized drug-rich nanoaggregates, experiments were performed with 10 mM FeSSIF. The micelle diameter in the blank media (d_H = 6 nm) did not change significantly (d_H = 8 nm) after addition of amorphous GLB.

Hence, all results indicated that the high aqueous GLB concentrations measured during ASD dissolution were not due to the presence of drug-rich nanoaggregates.

4. Discussion

4.1. Effect of polymer M_w on solid-state stability and drug dissolution from ASD

Several recent studies have investigated the effect of HPC M_w on the solid-state stability of ASD and on the stabilization of supersaturated drug solutions (Luebbert et al., 2021; Niederquell et al., 2022). In terms of the solid-state stability of ASD, lower M_w HPC polymers were shown to be superior to their higher M_w counterparts (Luebbert et al., 2021), in contrast to PVP which demonstrated a superior performance of its higher M_w species in respect to both stabilizing the amorphous state of ASDs and sustaining supersaturated drug solutions (Kestur, 2010; Mohapatra, 2017; Knopp, 2015).

The experimental results presented in the current paper did not show a significant effect of polymer M_w on the solid-state stability during storage of ASD formulations with 25 % GLB drug load (Fig. 2B): the formulations stabilized with HPC SSL and L were stable during the 4-months storage time, in contrast to the polymer-free SD-G. In contrast, dissolution experiments in biorelevant media showed that while all HPC polymers prevented drug precipitation, aqueous drug concentrations increased at lower HPC M_w, following the dependence SSL > L > M (Figs. 4 and 5).

Drug-rich nanoaggregates were not detected in the filtered aqueous phase (section 3.3.3). Considering the highly hydrophobic nature of GLB ($cLogD_{6.5}$ = 3.13), its molecules were most likely associated with the bile salt-phospholipid micelles (e.g. forming supersaturated micelles), rather than remaining as single, hydrated entities in the biorelevant media.

4.2. Mechanisms of the polymer M_w effect

Experiments with a physical mixture of GLB and HPC SSL (Figure S4 in the Supporting information), as well as pre-dissolving HPC polymers in the gastric fluids and adding amorphous GLB (Figs. 5 and 9), showed clearly that the high aqueous GLB concentrations generated by the ASDs were not due to drug-polymer interactions in the solid state. This was further confirmed by a series of ^{13}C solid-state NMR measurements, which demonstrated consistent chemical shifts of GLB and HPC SSL signals when comparing a physical mixture of amorphous GLB and HPC SSL to the corresponding spray-dried material (see Figures S7-S9 in the Supporting information).

Therefore, the impact of polymer on supersaturation stability and amorphous-to-crystalline transition of the dissolving solids will be discussed in the current section in light of their connection with the aqueous GLB concentrations. While these two processes may be linked, it has to be stressed that their nature is different. Supersaturation stability refers to the chemical potential gradient which drives the transfer of supersaturated drug molecules from the bulk aqueous phase to a solid phase by nucleation and/or crystal growth (Sarode, 2014; Taylor and Zhang, 2016; Lu, 2017; Quilló, 2021). On the other hand, the amorphous-to-crystalline transition of the drug or formulation solids is a solid-state phenomenon, which governs the amount of drug available for dissolution (Yoshioka et al., 1994; Alhalaweh, 2015; Shekunov, 2020; Wang and Sun, 2019). Hence, they will be discussed separately below.

4.2.1. Supersaturation stability

In presence of HPC polymers, the experimental dissolution profiles at intestinal conditions show gradually increasing aqueous drug concentrations, which are orders of magnitude higher than the reference crystalline drug solubility (Figs. 4 and 5). Therefore, all studied HPC grades successfully inhibit drug precipitation and provide high stability of the supersaturated solutions in the 2-hour time frame of the intestinal phase of the experiment. Hence, the effect of polymer M_w cannot be explained by a difference in the precipitation inhibition performance of the studied HPCs.

4.2.2. Dissolution and amorphous-to-crystalline transition

Series of model experiments (section 3.3) showed that the competition between crystallization and dissolution of the amorphous solids, and specifically the relative kinetics of the two processes determine the aqueous drug concentrations. Polymer M_w, intestinal colloids (bile salts and phospholipids) and pH were all found to influence these processes and the sum of their contributions controls the behaviour of the system. Each of the factors and their action are described below.

HPC polymers were found to decrease the rate of crystallization, effectively stabilizing the amorphous GLB particles at both gastric (Fig. 6) and intestinal conditions (Fig. 9B), as shown by DSC and WAXS measurements of the undissolved solids. Amorphous state stabilization was enhanced with decreasing the M_w of the polymer: [SSL, 40 kDa] > [L, 140 kDa] > [M, 700 kDa], in agreement with the ranking observed in the dissolution experiments (Figs. 4 and 5). The molecular mechanism of polymer action is discussed in the following section.

Intestinal colloids, *i.e.* bile salts and phospholipids, were found to act mainly by increasing the dissolution rate of the amorphous solids. This was most likely accomplished by a combination of improved penetration of water in the solids (wetting effect) and micellar solubilization (increased driving force for dissolution). This hypothesis was confirmed by using a combination of a conventional surfactant (1 % SDS) and a polymer (HPC SSL) at gastric conditions, which resulted at high aqueous drug concentrations even at low pH (section 3.3.1, last two paragraphs). A secondary effect linked to inhibition of amorphous-to-crystalline transition may also play a role (Chen, 2015), as indicated by the slower crystallization in presence of bile salts and phospholipids (Fig. 10), compared to the pure buffer system (Fig. 11). However, further experiments are required to validate this hypothesis.

An additional driving force for dissolution of amorphous GLB solids was found to be pH. Notably, GLB concentrations at gastric conditions (pH = 1.3) were below the detection limit of the analytical protocol, although the solids remained amorphous for 30 min when HPC SSL was present. At intestinal conditions (pH = 6.5 – 7.0), the partially ionized GLB dissolved rapidly when HPC SSL was present to stabilize the amorphous state of the solids (Fig. 5). When introduced in pure buffer at pH = 6.5, the transition of the solids from amorphous to crystalline state was faster than dissolution (Fig. 11), resulting in very low aqueous GLB concentrations. Further increase of pH to 9.5 resulted in dissolution outpacing crystallization even in pure buffer (Fig. 12), confirming the key effect of pH as a driver for high aqueous GLB concentrations at intestinal conditions.

The above results are in agreement with the effect of pH on the dissolution of ASD which has been recently discussed in the literature (Nguyen et al., 2023; Chiang, 2023; Almotairy, 2021). Interplay

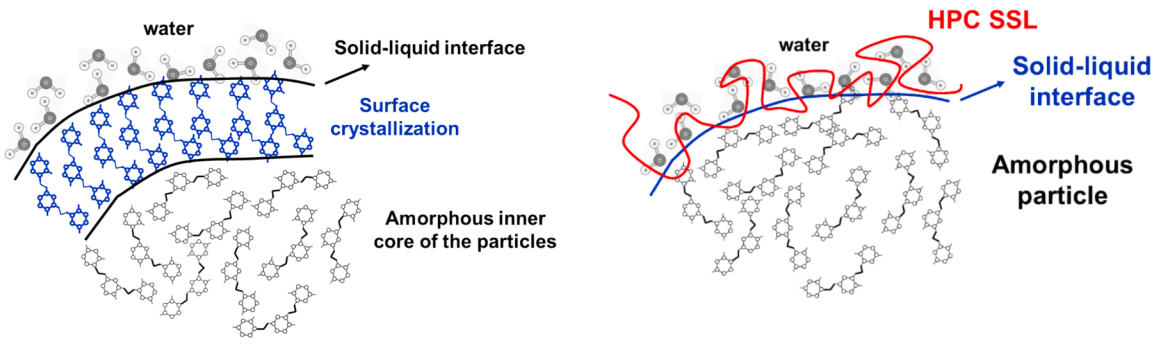

Fig. 13. Schematic illustration of the surface-induced crystallization of GLB solids (left hand side) and the inhibitory effect of the adsorbed polymer (right hand side).

between gastric pH and enteric polymers was shown to result in surface crystallization in some cases (Nguyen et al., 2023), whereas switching either the bulk or surface pH to values at which the drug is charged increased significantly the dissolution rate.

Therefore, the mechanism of enhanced drug dissolution from HPC-based amorphous GLB formulations is the inhibition of amorphous-to-crystalline transition during drug dissolution (Alonzo, 2010; Purohit, 2019; Savolainen, 2009), where HPC with lower M_w are more efficient in keeping a higher amorphous drug fraction which results in higher aqueous drug concentrations.

4.2.3. Molecular mechanism of amorphous state stabilization by HPC polymers

Having established that HPC polymers inhibit the amorphous-to-crystalline transition of the solid particles in biorelevant media, the molecular mechanisms underlying this process can be discussed. In situ observations of the process showed that the gradual conversion of amorphous particles to the crystalline state starts from particles that are found on the outer surface of particle aggregates, rather from inside of the particle aggregate (Fig. 7). Therefore, the transition seems to be driven by the contact between the aqueous media and the surface of the amorphous particles, following a heterogenous, surface nucleation pathway, as illustrated in Fig. 13. Observations that crystallization is more pronounced in smaller particles (compared to bigger aggregates) demonstrate a surface area-to-volume ratio effect which further supports the proposed surface nucleation mechanism (Dyett, 2018; Jung, 2012; Li, 2012; Seddon, 2016; Denkov et al., 2019; Cholakova and Denkov, 2023; Cholakova, 2023).

If the amorphous-to-crystalline transition of GLB particles in biorelevant media is driven by the described surface nucleation mechanism, the link between HPC M_w and crystallization inhibition can be rationalized. Lower M_w HPC will adsorb much more quickly (compared to the higher M_w species) on the surface of the amorphous GLB particles due to its faster diffusion, which is critical, considering the fast amorphous-to-crystalline transition (first crystals observed after 1 min in a static experiment, Fig. 7), and the competition between crystallization and dissolution.

Once adsorbed, the polymer chain will disturb the packing and orientation of the drug molecules on the surface, significantly decreasing the probability for nucleus formation. Additionally, the shorter chain of the lower M_w polymer species may insert more easily between neighbouring drug molecules on the particle surface, further increasing the crystallization inhibition performance, compared to the higher M_w polymers. The higher surface activity and surfactant-like properties of lower M_w HPC, which has been recently reported, supports this explanation (Niederquell et al., 2022), as well as the crystallization inhibition effect of bile salts observed in the current study (Fig. 10). Experimental data for ice crystallization has shown that the orientation and mobility of the molecules on the surface of a crystallizing material play an important role in the nucleation and crystallization process (Seddon, 2016).

Having clarified the molecular mechanism of stabilization of the amorphous state of GLB by HPC polymers, it is of interest to discuss the generality of the effect. It would be reasonable to assume that HPC polymers and other crystallization inhibitors will be able to stabilize the amorphous state of drug molecules, which crystallize via the surface-induced nucleation mechanism. It has been established that such molecules are characterized by high surface mobility, which is linked to lower molecular weight and weaker hydrogen bond interactions (Chen et al., 2016; Huang, 2017; Huang, 2017; Zhang and Yu, 2016). However, further studies have to be performed in order to validate this hypothesis.

5. Conclusions

The effect of HPC polymers M_w on the stability and dissolution performance of GLB solid dispersions in biorelevant dissolution media was studied and the mechanisms underlying the observed effects were discussed. It was revealed that during dissolution, HPC polymers inhibit the experimentally observed amorphous-to-crystalline transition by preventing surface-induced nucleation. The link between polymer M_w and performance was rationalized by considering the faster diffusion, higher surface activity and better ability to disrupt the packing of drug molecules on the particle surface of the lower M_w HPC SSL, compared to the higher M_w HPC analogues, which inhibited drug crystallization to a smaller extent. However, aqueous drug concentrations were shown to be governed not only by the solid-state stability in solution, but also by the interplay between wetting, solubilization and pH. These new insights into the molecular mechanisms of ASD dissolution suggest that polymer surface activity and rate of adsorption may be an important parameter when drug solid-state stability during dissolution is governed by surface nucleation, and that pH effects must also be considered in relation to the competitive kinetics of crystallization and dissolution.

CRediT authorship contribution statement

Vladimir Petkov: Writing – original draft, Visualization, Resources, Methodology, Investigation. **Zahari Vinarov:** Writing – review & editing, Supervision, Resources, Project administration, Methodology, Funding acquisition, Conceptualization. **Slavka Tcholakova:** Writing – review & editing, Supervision, Resources, Funding acquisition, Conceptualization.

Declaration of competing interest

The authors declare the following financial interests/personal relationships which may be considered as potential competing interests: Zahari Vinarov reports financial support was provided by Bulgarian National Science Fund. Vladimir Petkov reports equipment, drugs, or supplies was provided by European Union. Slavka Tcholakova reports financial support was provided by European Union. If there are other authors, they declare that they have no known competing financial interests or personal relationships that could have appeared to influence

the work reported in this paper.

Acknowledgments

The authors acknowledge Operational Program" Science and Education for Smart Growth" 2014–2020, co-financed by European Union through the European Structural and Investment Funds, Grant BG05M2OP001-1.002-0012 "Sustainable Utilization of Bio-resources and Waste of Medicinal and Aromatic Plants for Innovative Bioactive Products" for providing access to research infrastructure. Z.V. gratefully acknowledges the support of the Bulgarian Ministry of Education and Science, under the National Research Program "VIHREN-2021", project 3D-GUT (№ KP-06-DV-3/15.12.2021). S.T. gratefully acknowledges the support of European Union-Next Generation EU, through the National Recovery and Resilience Plan of the Republic of Bulgaria, project № BG-RRP-2.004-0008-C01. The authors are grateful to Edmont Stoyanov and Nisso GmbH for supplying the HPC polymers used in the study. The assistance of Dr. Sonya Tsibranska with the initial experiments, Dr. Zlatina Mitrinova with the WAXS measurements, of Dr. Lyuben Mihaylov and Dr. Evelina Vassileva with the cryo-TEM imaging, and of Dr. Gazolu-Rusanova with the contact angle measurements is also gratefully acknowledged.

Appendix A. Supplementary data

Supplementary data to this article can be found online at https://doi.org/10.1016/j.ijpharm.2024.124820.

Data availability

Data will be made available on request.

References

Alhalaweh, A., et al., 2015. Physical stability of drugs after storage above and below the glass transition temperature: Relationship to glass-forming ability. Int. J. Pharm. 495 (1), 312–317.
Almotairy, A., et al., 2021. Effect of pH Modifiers on the solubility, dissolution rate, and stability of telmisartan solid dispersions produced by hot-melt extrusion technology. J. Drug. Deliv. Sci. Technol 65.
Alonzo, D.E., et al., 2010. Understanding the behavior of amorphous pharmaceutical systems during dissolution. Pharm. Res 27 (4), 608–618.
Alonzo, D.E., et al., 2011. Dissolution and precipitation behavior of amorphous solid dispersions. J. Pharm. Sci 100 (8), 3316–3331.
Boyd, B.J., et al., 2019. Successful oral delivery of poorly water-soluble drugs both depends on the intraluminal behavior of drugs and of appropriate advanced drug delivery systems. Eur. J. Pharm. Sci 137, 104967.
Butreddy, A., 2022. Hydroxypropyl methylcellulose acetate succinate as an exceptional polymer for amorphous solid dispersion formulations: A review from bench to clinic. Eur. J. Pharm. Biopharm.
Butreddy, A., et al., 2022. Hot-melt extruded hydroxypropyl methylcellulose acetate succinate based amorphous solid dispersions: Impact of polymeric combinations on supersaturation kinetics and dissolution performance. Int. J. Pharm. 615, 121471.
Chavan, R.B., et al., 2019. Cellulose based polymers in development of amorphous solid dispersions. Asian. J. Pharm. Sci. 14 (3), 248–264.
Chavan, R.B., Lodagekar, A., Shastri, N.R., 2018. Determination of precipitation inhibitory potential of polymers from amorphous solid dispersions. Drug. Devel. Industr. Pharm. 44 (12), 1933–1941.
Chen, J., et al., 2015. Bile salts as crystallization inhibitors of supersaturated solutions of poorly water-soluble compounds. Cryst. Growth. Des. 15 (6), 2593–2597.
Chen, Y., Zhang, W., Yu, L., 2016. Hydrogen bonding slows down surface diffusion of molecular glasses. J. Phys. Chem. B 120 (32), 8007–8015.
Chiang, C.W., et al., 2023. Effect of buffer pH and concentration on the dissolution rates of sodium indomethacin-copovidone and indomethacin-copovidone amorphous solid dispersions. Mol. Pharm 20 (12), 6451–6462.
Cholakova, D., et al., 2023. Structure of rotator phases formed in C13–C21 alkanes and their mixtures. in bulk and in emulsion drops. Cryst. Growth. Des. 24 (1), 362–377.
Cholakova, D., Denkov, N., 2023. Polymorphic phase transitions in triglycerides and their mixtures studied by SAXS/WAXS techniques: In bulk and in emulsions. Adv. Colloid. Interface. Sci., 103071
Corrie, L., et al., 2023. HPMCAS-based amorphous solid dispersions in clinic: A review on manufacturing techniques (Hot Melt Extrusion and Spray Drying), marketed products and patents. Materials 16 (20), 6616.
Dedroog, S., Huygens, C., Van den Mooter, G., 2019. Chemically identical but physically different: A comparison of spray drying, hot melt extrusion and cryo-milling for the formulation of high drug loaded amorphous solid dispersions of naproxen. Eur. J. Pharm. Biopharm 135, 1–12.
Denkov, N., Tcholakova, S., Cholakova, D., 2019. Surface phase transitions in foams and emulsions. Curr. Opin. Colloid. Interface. Sci. 44, 32–47.
Dyett, B., et al., 2018. Crystallization of femtoliter surface droplet arrays revealed by synchrotron small-angle X-ray scattering. Langmuir 34 (32), 9470–9476.
Fuchs, A., et al., 2015. Advances in the design of fasted state simulating intestinal fluids: FaSSIF-V3. Eur. J. Pharm. Biopharm. 94, 229–240.
Grohganz, H., et al., 2014. Refining stability and dissolution rate of amorphous drug formulations. Expert. Opin. Drug. Deliv 11 (6), 977–989.
Hassan, M.A., et al., 1997. Preparation and characterization of a new polymorphic form and a solvate of glibenclamide. Acta. Pharm. Hung 67 (2–3), 81–88.
Huang, C., et al., 2017. Effect of low-concentration polymers on crystal growth in molecular glasses: A controlling role for polymer segmental mobility relative to host dynamics. J. Physi. Chemi. B 121 (8), 1963–1971.
Huang, C., et al., 2017. Fast surface diffusion and crystallization of amorphous griseofulvin. J. Phys. Chem. B 121 (40), 9463–9468.
Jung, S., et al., 2012. Mechanism of supercooled droplet freezing on surfaces. Nat. Commun 3, 615.
Kestur, U.S., et al., 2010. Effects of the molecular weight and concentration of polymer additives, and temperature on the melt crystallization kinetics of a small drug molecule. Cryst. Growth. Des. 10 (8), 3585–3595.
Knopp, M.M., et al., 2015. Influence of polymer molecular weight on drug-polymer solubility: A comparison between experimentally determined solubility in PVP and prediction derived from solubility in monomer. J. Pharm. Sci 104 (9), 2905–2912.
Knopp, M.M., et al., 2016. Effect of polymer type and drug dose on the in vitro and in vivo behavior of amorphous solid dispersions. Eur. J. Pharm. Biopharm 105, 106–114.
Konno, H., et al., 2008. Effect of polymer type on the dissolution profile of amorphous solid dispersions containing felodipine. Eur. J. Pharm. Biopharm 70 (2), 493–499.
Konno, H., Taylor, L.S., 2006. Influence of different polymers on the crystallization tendency of molecularly dispersed amorphous felodipine. J. Pharm. Sci 95 (12), 2692–2705.
Laitinen, R., et al., 2013. Emerging trends in the stabilization of amorphous drugs. Int. J. Pharm 453 (1), 65–79.
Li, C.L., et al., 2010. The use of hypromellose in oral drug delivery. J. Pharm. Pharmacol. 57 (5), 533–546.
Li, K., et al., 2012. Investigating the effects of solid surfaces on ice nucleation. Langmuir 28 (29), 10749–10754.
Lu, J., et al., 2017. Maintaining Supersaturation of active pharmaceutical ingredient solutions with biologically relevant bile salts. Cryst. Growth. Des. 17 (5), 2782–2791.
Luebbert, C., Stoyanov, E., Sadowski, G., 2021. Phase behavior of ASDs based on hydroxypropyl cellulose. Int. J. Pharm. X 3, 100070.
Mohapatra, S., et al., 2017. Effect of polymer molecular weight on the crystallization behavior of indomethacin amorphous solid dispersions. Cryst. Growth. Des. 17 (6), 3142–3150.
Mukesh, S., et al., 2023. Comparative analysis of drug-salt-polymer interactions by experiment and molecular simulation improves biopharmaceutical performance. Commun. Chem. 6 (1), 201.
Nguyen, H.T., Van Duong, T., Taylor, L.S., 2023. Impact of gastric pH variations on the release of amorphous solid dispersion formulations containing a weakly basic drug and enteric polymers. Mol. Pharm 20 (3), 1681–1695.
Niederquell, A., Stoyanov, E., Kuentz, M., 2022. Hydroxypropyl cellulose for drug precipitation inhibition: from the potential of molecular interactions to performance considering microrheology. Mol. Pharm 19 (2), 690–703.
Panagopoulou-Kaplani, A., Malamataris, S., 2000. Preparation and characterisation of a new insoluble polymorphic form of glibenclamide. Int. J. Pharm. 195 (1), 239–246.
Purohit, H.S., et al., 2019. Assessing the impact of endogenously derived crystalline drug on the in vivo performance of amorphous formulations. Mol. Pharm. 16 (8), 3617–3625.
Quilló, G.L., et al., 2021. Crystal growth kinetics of an industrial active pharmaceutical ingredient: implications of different representations of supersaturation and simultaneous growth mechanisms. Cryst. Growth. Des. 21 (9), 5403–5420.
Sanz, D., et al., 2012. The structure of glibenclamide in the solid state. Magnetic. Resonance. Chem. 50 (3), 246–255.
Sarode, A.L., et al., 2014. Supersaturation, nucleation, and crystal growth during single- and biphasic dissolution of amorphous solid dispersions: polymer effects and implications for oral bioavailability enhancement of poorly water soluble drugs. Eur. J. Pharm. Biopharm 86 (3), 351–360.
Savolainen, M., et al., 2009. Better understanding of dissolution behaviour of amorphous drugs by in situ solid-state analysis using Raman spectroscopy. Eur. J. Pharm. Biopharm. 71 (1), 71–79.
Seddon, A.M., et al., 2016. Control of Nanomaterial Self-Assembly in Ultrasonically Levitated Droplets. J. Phys. Chem. Lett 7 (7), 1341–1345.
Shan, X., et al., 2021. Mutual effects of hydrogen bonding and polymer hydrophobicity on ibuprofen crystal inhibition in solid dispersions with poly(N-vinyl pyrrolidone) and poly(2-oxazolines). Pharmaceutics 13 (5).
Shekunov, B., 2020. Kinetics of Crystallization and Glass Transition in Amorphous Materials. Cryst. Growth. Des. 20 (1), 95–106.
Singh, A., Van den Mooter, G., 2016. Spray drying formulation of amorphous solid dispersions. Adv. Drug. Deliv. Rev 100, 27–50.
Sterren, V.B., et al., 2021. Enhanced dissolution profiles of glibenclamide with amino acids using a cogrinding method. Mater. Today. Commun. 26, 102126.
Suleiman, M.S., Najib, N.M., 1989. Isolation and physicochemical characterization of solid forms of glibenclamide. Int. J. Pharm. 50 (2), 103–109.

Taylor, L.S., Zhang, G.G.Z., 2016. Physical chemistry of supersaturated solutions and implications for oral absorption. Adv. Drug. Deliv. Rev 101, 122–142.
Vinarov, Z., et al., 2012. In vitro study of triglyceride lipolysis and phase distribution of the reaction products and cholesterol: effects of calcium and bicarbonate. Food. Funct. 3 (11), 1206–1220.
Wang, K., Sun, C.C., 2019. Crystal growth of celecoxib from amorphous state: polymorphism, growth mechanism, and kinetics. Cryst. Growth. Des. 19 (6), 3592–3600.
Wu, J., Mooter, G.V.D., 2023. The influence of hydrogen bonding between different crystallization tendency drugs and PVPVA on the stability of amorphous solid dispersions. Int. J. Pharm 646, 123440.
Yoshioka, M., Hancock, B.C., Zografi, G., 1994. Crystallization of indomethacin from the amorphous state below and above its glass transition temperature. J. Pharm. Sci. 83 (12), 1700–1705.
Zangenberg, N.H., et al., 2001. A dynamic in vitro lipolysis model. I. Controlling the rate of lipolysis by continuous addition of calcium. Eur. J. Pharm. Sci 14 (2), 115–122.
Zhang, W., Yu, L., 2016. Surface diffusion of polymer glasses. Macromolecules 49 (2), 731–735.